

Quantum threshold reflection is not a consequence of a region of the long-range attractive potential with rapidly varying de Broglie wavelength

Jakob Petersen^{*} and Eli Pollak[†]

Department of Chemical and Biological Physics, Weizmann Institute of Science, 76100 Rehovot, Israel

Salvador Miret-Artes[‡]

Instituto de Física Fundamental, CSIC, Serrano 123, 28006 Madrid, Spain



(Received 25 October 2017; revised manuscript received 7 December 2017; published 3 April 2018)

Quantum threshold reflection is a well-known quantum phenomenon which prescribes that at threshold, except for special circumstances, a quantum particle scattering from any potential, even if attractive at long range, will be reflected with unit probability. In the past, this property had been associated with the so-called badlands region of the potential, where the semiclassical description of the scattering fails due to a rapid spatial variation of the de Broglie wavelength. This badlands region occurs far from the strong interaction region of the potential and has therefore been used to “explain” the quantum reflection phenomenon. In this paper we show that the badlands region of the interaction potential is immaterial. The extremely long wavelength of the scattered particle at threshold is much longer than the spatial extension of the badlands region, which therefore does not affect the scattering. For this purpose, we review and generalize the proof for the existence of quantum threshold reflection to stress that it is only a consequence of continuity and boundary conditions. The nonlocal character of the scattering implies that the whole interaction potential is involved in the phenomenon. We then provide a detailed numerical study of the threshold scattering of a particle by a Morse potential and an Eckart potential, especially in the time domain. We compare exact quantum computations with incoherent results obtained from a classical Wigner approximation. This study shows that close to threshold the time-dependent amplitude of the scattered particle is negligible in the badlands region and is the same whether the potential has a reflecting wall as in the Morse potential or a steplike structure as in the Eckart smooth step potential. The mean flight time of the particle is not shortened due to a local reflection from the badlands region or due to the lower density of the wave function at short distances. This study should serve to definitely rule out the badlands region as a qualitative guide to the properties of quantum threshold reflection.

DOI: [10.1103/PhysRevA.97.042102](https://doi.org/10.1103/PhysRevA.97.042102)

I. INTRODUCTION

In any standard quantum mechanics textbook, one of the first elementary exercises proposed for one-dimensional potentials is the reflection by a step potential. When the energy of the incident particle is greater than the step, the initial wave function is reflected and transmitted at the discontinuity point of the potential. At threshold conditions, where the incident energy approaches the step height, the reflection probability tends to one. This condition is termed total (quantum) reflection since the transmitted part of the initial wave function is totally suppressed and no classical turning point is present. Senn [1] established a theorem for general one-dimensional potentials which vanish as the coordinate goes to $\pm\infty$, showing that the reflection probability goes to unity at threshold conditions except under the special circumstance that the potential supports a resonance state at threshold.

Threshold conditions and/or laws are of paramount importance in gas-phase collisions and scattering of atoms by

solid surfaces. When the incident energy is close to zero, the corresponding de Broglie wavelength tends to infinity as the inverse of the square root of the energy and quantum effects are expected to be critical. Lennard-Jones and Devonshire [2] first recognized this behavior in the context of atom-surface interaction. Kohn [3] subsequently showed that quantum reflection leads to a zero sticking probability in threshold particle surface scattering. As Kohn pointed out, “it is clearly a quantum interference effect between the incoming and reflected waves.” Quantum threshold reflection prevents sticking since atoms are not able to come into contact with the surface. The same phenomenon was reported by Côté *et al.* [4] in cold-atom collisions, although the authors preferred to name it quantum suppression since suppression entails some sort of exclusion of amplitude from certain regions. These authors also realized that one of the exceptions to the suppression is the presence of a bound state at threshold with no mention of Senn’s work, which surprisingly has been overlooked for years in this context.

Most of the theoretical work in this field has been carried out using the semiclassical WKB framework [5,6] since analytical expressions are readily obtained. Within the primitive WKB theory, reflection is only possible if there exist classical trajectories which are reflected by the potential. Therefore, necessarily, quantum reflection, especially for a purely

^{*}jakob.petersen@weizmann.ac.il

[†]eli.pollak@weizmann.ac.il

[‡]s.miret@iff.csic.es

attractive potential, cannot be described by WKB theory (unless one includes higher-order corrections or connection formulas). With this perspective, Friedrich and Trost [6] conclude the following: “Quantum reflection can only occur in a region of appreciable quantality, i.e. where the condition (36) is violated.” The condition (36) they mention refers to the badlands function (also known as the quantality function) defined in Eq. (3.19) below, which is related to the rapidity of the spatial change of the de Broglie wavelength, which must remain small for the WKB approximation to be valid.

At near-threshold conditions, the quantality function becomes very large in a finite spatial region which is quite far from the surface, where the actual attractive force on the particle is very weak. Friedrich *et al.* assume that the quantum reflection emanates from this badlands region [6–8]. In Ref. [9] Friedrich writes: “even though there is no potential barrier and no classical turning point, incoming waves can be partially reflected in this nonclassical region of coordinate space, so that only a fraction of the incoming radial wave penetrates through to the near-origin regime. Such classically forbidden reflection. . . is called *quantum reflection*.”

In Ref. [8], Friedrich and Jurisch note that “this nonclassical region is typically located at distances of several hundreds or thousands of atomic units where the potentials are well described by van der Waals forces with retardation effects.” In their view, the failure of the WKB approximation in this region provides a local condition for quantum reflection since it is restricted to occur in a small part of the coordinate space. This qualitative picture is widely used and accepted. Stickler *et al.* [10] comment that “where $B(y)$ is significantly nonzero can be regarded as regions where quantum reflection can occur” [$B(y)$ indicates the badlands function]. For example, in their recent measurements on electrically controlled quantum reflection, Barnea *et al.* [11] note in their Fig. 2 that “the inset shows the badlands function for different voltages, indicating the region contributing to quantum reflection.”

As mentioned, for example, by Doak and Chizmeshya [12], the WKB approximation breaks down in the region where the magnitude of the attractive potential energy equals the incident energy. They then note the following: “In a sense, this region can be viewed as an analog at positive kinetic energy to a classical turning point.” Mody *et al.* [5] claim the same, stating the following: “The distance away from the slab at which the particle is turned around—or quantum reflected—is precisely this distance.” Zhang *et al.* [13] point out in the legend to their Fig. 1, which is meant to describe the general phenomenon of quantum reflection, that “[the] quantum reflection probability is [nonvanishing] in a range of distances around z_0 defined as the distance where the absolute magnitude of the potential energy $|V(z_0)|$ equals the incident kinetic energy E_z .”

We do not question the fact that the region in which the WKB approximation breaks down is local and reasonably well defined by the region in which the badlands function is greater than unity or that equivalently the incident kinetic energy is the same as the magnitude of the attractive long-range potential. Nor do we question the interesting observation of Dufour *et al.* [14,15], that the badlands region creates an effective potential barrier for the action of the particle. However, this does not mean that the wave function of the particle is locally reflected by this region. In a recent paper [16], the

close-coupling formalism (which is numerically exact when convergence is reached) has been used successfully to describe the experimental work on the quantum reflection of He atoms from a grating [17,18]. The interaction potential consisted of two parts, the long range was given by a Casimir–van der Waals tail and the short range by a Morse potential. In order to avoid the left classical turning point of the repulsive part of the Morse potential which also leads to reflection and so makes it difficult to distinguish it from the long-range quantum reflection, absorbing boundary conditions were used [19,20]. This was implemented by introducing an imaginary potential which is essentially zero in the physically relevant interaction region and is turned on at the edge of the coordinate grid for numerical integration, preventing reflection from the repulsive part of the potential. The central conclusion of Ref. [16] was that quantum reflection is a coherent interference process which involves the full interaction potential. It should be considered as a *nonlocal effect*. Furthermore, in this formalism, the dynamics takes place among the different (diffraction) channels needed for numerical convergence. The picture that emerged from our previous computation was that at near-threshold conditions, quantum reflection was a nonlocal coherent process.

The purpose of the work presented here is to resolve this issue once and for all. We will show that the quantum wave function is not locally reflected by the badlands region of the attractive part of the potential. As its name states, quantum reflection is a quantum effect; one proves its existence without the need to resort to any semiclassical theory or to the badlands function. For this purpose we find it necessary to review and generalize, in Sec. II, Senn’s proof of quantum threshold reflection in one-dimensional systems. We review the proof for the case of a potential that vanishes at $\pm\infty$ but consider also the case of a repulsive potential which goes to ∞ such as the Morse potential as well as the case of asymmetric asymptotic potentials. In all of these one finds threshold quantum reflection which is a direct result of boundary conditions and continuity of the wave function and its derivative. It is thus a global effect and very general. The potential plays a role in determining how small the incident kinetic energy must be for quantum reflection to become important.

We also note that to date, although quantum time-dependent computations in the context of quantum reflection abound (see, for example, Refs. [21,22]), no one has undertaken such a computation to follow the wave packet in time to see where and whether it is reflected. This is not an accident; due to the very low energies involved, one needs to evolve a wave packet which is very broad in space and moves very slowly. This is difficult to implement, using numerical wave-packet propagation techniques, even with present-day computational resources. However, if the propagator is known analytically, the problem becomes much easier.

For this purpose, we present in Sec. III a detailed study of the quantum reflection phenomenon for a particle scattered on a Morse potential. We derive an explicit expression for the propagator and use it to study the space and time dependence of the scattering dynamics of the Morse potential at low incident momenta where quantum threshold reflection dominates the dynamics.

Since the tail of the Morse potential is exponential, it has a badlands region and so may be used to study in detail its

impact on the scattering. We find that indeed, due to the very long wavelength of the incident particle at the ultralow energies leading to quantum threshold reflection, the large fraction of the density of the particle at all times stays far away from the origin where the Morse potential has its well. The lower the energy, the further away the density stays from the origin. However, we show that this distance has nothing to do with the badlands region of the potential; it is just due to the long wavelength and the sine form of the wave packet in the region where quantum reflection is dominant. We repeat such a computation using also an Eckart step potential and find the same. In fact, at very low energies where the quantum reflection probability is close to unity, the time-dependent wave function for the Eckart step potential is indistinguishable from the one found for the Morse potential.

To complete the picture, we also consider the time associated with quantum reflection. We compare the quantum coherent time-dependent dynamics with an approximation based on what is known in the chemistry literature as a classical Wigner approximation [23,24] whereby one uses the quantum form of the incident Gaussian wave function in phase space as represented by its Wigner representation, but the time evolution is carried out using classical mechanics. This classical Wigner approximation presents an incoherent approximation to the quantum dynamics. As also found using other methods [8], the classical Wigner flight time associated with the reflection is found to be slightly *shorter* than the quantum flight time as determined from the mean quantum transition path time. This is but another indication that one should not think of the quantum particle as being reflected far away from the surface, for if this were the case, the quantum flight time would have to be much shorter than that determined from a classical Wigner approximation. In contrast to the expectation based on considering the residence time of the particle in the interaction region [25], the quantum flight time is *longer* than the classical time, even though the density of the classically propagated Wigner distribution in the strong interaction region of the potential is much larger than that of the exact quantal density. At low energies, the quantum density is noticeable only far away from the surface, at a distance comparable to its de Broglie wavelength, while the density generated through the Wigner dynamics does have appreciable amplitude close to the surface.

This nicely demonstrates Kohn's prediction [3] that although classically the sticking coefficient at threshold is unity, the quantum coefficient vanishes due to quantum reflection, which prevents any noticeable amplitude of the wave function close to the surface. It is also consistent with the observation that He dimers do not dissociate upon quantum reflection [18], since the density of the dimers is always sufficiently far from the surface to prevent any interaction which would break up the ultraweak bond. We end in Sec. IV with a discussion of the implications of the present study on quantum threshold surface scattering.

II. QUANTUM REFLECTION FOR GENERAL INTERACTION POTENTIALS

Senn [1] established a quantum reflection theorem for one-dimensional scattering. He considered the specific case

in which the potential vanishes in the limits $x \rightarrow \pm\infty$. He showed that the portion of particles that is transmitted in general vanishes as the kinetic energy of the incident particles approaches zero. He also showed that this behavior is no longer valid when a bound level is present at the onset of the continuum and in such cases, the reflection coefficient, even at threshold, is less than unity. In particular, for symmetric potentials, the resonance condition implies that the reflection coefficient vanishes at threshold (threshold anomalies). In this section we will review his proof and generalize it to two further cases: one in which the potential has a repulsive wall, the other in the case of an asymmetric potential whose asymptotic energy at $x \rightarrow \infty$ differs from its asymptotic energy as $x \rightarrow -\infty$. We will refer to this case as an asymmetric asymptotic potential. It is very instructive to review his derivation since it lies at the heart of understanding the quantum threshold reflection phenomenon.

A. Symmetric asymptotic potential

We consider a particle with mass m , coordinate x , and incident momentum $\hbar k$ with $k > 0$. We first assume that the potential $V(x)$ differs appreciably from zero only inside a finite interval for which $-\xi < x < \xi$. Let u and v denote two linearly independent solutions of the corresponding one-dimensional Schrödinger equation. For a particle incident from the left with positive momentum ($\hbar k$), the wave function is

$$\Psi(x) = T(k) \exp(ikx) \quad (2.1)$$

for $x \geq \xi$ and

$$\Psi(x) = \exp(ikx) + R(k) \exp(-ikx) \quad (2.2)$$

for $x \leq -\xi$, where $T(k)$ and $R(k)$ are the transmission and reflection amplitudes, respectively. Inside the region where the potential is different from zero, the wave function can be written as

$$\Psi(x) = au(x) + bv(x), \quad (2.3)$$

where the following boundary conditions are chosen to ensure independence of the two solutions:

$$v(-\xi) = u'(-\xi) = 0, \quad u(-\xi) = v'(-\xi) = 1. \quad (2.4)$$

These boundary conditions imply that the Wronskian of u and v denoted by $W(u,v) = uv' - u'v$ is unity.

In addition to the boundary conditions one must impose continuity of the wave function Ψ and its first derivative at $x = \pm\xi$:

$$\begin{aligned} \exp(-ik\xi) + R(k) \exp(+ik\xi) &= a, \\ ik[\exp(-ik\xi) - R(k) \exp(+ik\xi)] &= b, \\ T(k) \exp(+ik\xi) &= au(\xi) + bv(\xi), \\ ikT(k) \exp(+ik\xi) &= au'(\xi) + bv'(\xi). \end{aligned} \quad (2.5)$$

This set of linear equations is readily solved to express the reflection amplitude in terms of the various values of the wave function and its first derivative:

$$R(k) = \exp(-2ik\xi) \frac{k(p-q) + i(sk^2 - w)}{k(p+q) + i(sk^2 + w)}, \quad (2.6)$$

where $p = v'(\xi)$, $q = u(\xi)$, $s = -v(\xi)$, and $w = u'(\xi)$. Similarly, using the Wronskian relationship $pq + ws = 1$, the transmission amplitude is found to be given by

$$T(k) = \frac{\exp(-2ik\xi)2k}{k(p+q) + i(sk^2 + w)}. \quad (2.7)$$

Thus, the reflection probability is given by

$$|R(k)|^2 = \frac{w^2 + k^2[(p-q)^2 - 2sw] + s^2k^4}{w^2 + k^2[(p+q)^2 + 2sw] + s^2k^4}. \quad (2.8)$$

In the limit that $k \rightarrow 0$ one finds that $|R|^2 \rightarrow 1$ unless w tends to zero as well. If $w \rightarrow 0$ then

$$\lim_{k, w \rightarrow 0} |R(k)|^2 = \frac{(p-q)^2}{(p+q)^2} \quad (2.9)$$

and the reflection coefficient at threshold will in general differ from unity unless p or q vanishes for $k \rightarrow 0$. The condition $w = 0$ in the limit $k \rightarrow 0$ holds if and only if the potential supports a bound state at $E = 0$. This proof is given in detail in Ref. [1]. For our purposes of studying quantum reflection, we will assume that $w \neq 0$. From Eqs. (2.6) and (2.7) we readily find that in the threshold limit

$$\begin{aligned} \lim_{k \rightarrow 0} T(k) &= -\exp(-2ik\xi) \frac{2ik}{w}, \\ \lim_{k \rightarrow 0} R(k) &= -\exp(-2ik\xi) \left[1 + \frac{2ikp}{w} \right], \end{aligned} \quad (2.10)$$

implying that the transmission amplitude vanishes linearly with diminishing k and the reflection amplitude goes to -1 .

B. Repulsive potential

The second case to be studied is when the potential goes to ∞ when $x \rightarrow \infty$ as in surface scattering. In this case the analysis is simplified, since the transmission coefficient vanishes or, in other words, we have the boundary condition that the wave function vanishes when we go far enough to positive values of the coordinate. The solution of Eqs. (2.5) simplifies to

$$R(k) = \exp(-2ik\xi) \frac{ks + iq}{ks - iq} \quad (2.11)$$

and quantum reflection takes the form (with $q \neq 0$)

$$\lim_{k \rightarrow 0} R(k) = -\exp(-2ik\xi) \left[1 - \frac{2iks}{q} \right]. \quad (2.12)$$

Quantum reflection in this case may be identified by noting that the imaginary part of the reflection amplitude becomes linear with k .

C. Asymmetric asymptotic potential

In this third scenario we assume that the potential $V(x)$ differs appreciably from a constant only inside a finite interval for which $-\xi < x < \xi$. For $x < -\xi$ we assume that the potential vanishes, while for $x > \xi$ the potential is $-V$ with $V > 0$. For an incident energy E we use the notation for the wave vectors k and k' as follows:

$$E = \frac{\hbar^2 k^2}{2m} = \frac{\hbar^2 k'^2}{2m} - V. \quad (2.13)$$

As before, we let u and v denote two linearly independent solutions of the corresponding one-dimensional Schrödinger equation. For a particle incident from the left with positive momentum ($\hbar k$), the wave function is

$$\Psi(x) = \sqrt{\frac{k}{k'}} T(k) \exp(ik'x) \quad (2.14)$$

for $x \geq \xi$ and

$$\Psi(x) = \exp(ikx) + R(k) \exp(-ikx) \quad (2.15)$$

for $x \leq -\xi$. Inside the region where the potential is different from zero, the wave function can be written as in Eq. (2.3) and the boundary conditions are chosen as in Eq. (2.4).

Imposing the continuity of the wave function Ψ and its first derivative at $x = \pm\xi$ implies

$$\begin{aligned} \exp(-ik\xi) + R(k) \exp(ik\xi) &= a, \\ ik[\exp(-ik\xi) - R(k) \exp(ik\xi)] &= b, \\ \sqrt{\frac{k}{k'}} T(k) \exp(ik'\xi) &= au(\xi) + bv(\xi), \\ i\sqrt{k'k} T(k) \exp(ik'\xi) &= au'(\xi) + bv'(\xi). \end{aligned} \quad (2.16)$$

This set of linear equations is readily solved. One finds that the reflection amplitude is

$$R(k) = \exp(-2ik\xi) \left[\frac{kp - k'q + i(sk'k' - w)}{kp + k'q + i(sk'k' + w)} \right]. \quad (2.17)$$

Here we used the same notation as before, that is, $p = v'(\xi)$, $q = u(\xi)$, $s = -v(\xi)$, and $w = u'(\xi)$. Similarly, the transmission amplitude is found to be

$$T(k) = \exp[-i(k+k')\xi] \left[\frac{2\sqrt{kk'}}{kp + k'q + i(sk'k' + w)} \right]. \quad (2.18)$$

It remains to consider the limit when the incident momentum vanishes. Using the notation

$$k_\infty = \sqrt{\frac{2mV}{\hbar^2}}, \quad (2.19)$$

one readily finds to first order in k for the reflection coefficient

$$\lim_{k \rightarrow 0} R(k) = \exp(-2ik\xi) \left[-1 + \frac{2k(p + isk_\infty)}{(k_\infty q + iw)} \right]. \quad (2.20)$$

This result is instructive. In contrast to the symmetric asymptotic potential case, here, even if $w = 0$, one still obtains the threshold reflection behavior, that is, the reflection amplitude goes to -1 at threshold. For the transmission coefficient one finds that

$$\lim_{k \rightarrow 0} T(k) = \exp[-i(k+k_\infty)\xi] \left[\frac{2\sqrt{kk_\infty}}{(iw + k_\infty q)} \right], \quad (2.21)$$

so as expected $\sqrt{\frac{k}{k'}} T(k)$ is linear in k in this limit.

One should also consider the case of an attractive potential in the sense that $V(x) \rightarrow -\infty$ as $x \rightarrow \infty$. This is though a limiting case of the asymmetric asymptotic potential for which $V \rightarrow \infty$. Since quantum reflection is found for any finite value of V , it will also hold in this limit of an attractive potential.

To summarize, as shown in all cases, quantum reflection, that is, a reflection amplitude which at threshold ($k \rightarrow 0$) goes to -1 , is universal and a result only of the continuity of the wave function and the boundary conditions. There is no need to consider a badlands region to explain the phenomenon.

III. QUANTUM REFLECTION FOR THE MORSE POTENTIAL

A. Energy domain: Scattering wave functions

In the preceding section, an analysis of the behavior of the reflection coefficient for a general one-dimensional potential was reviewed. The continuity requirement of the wave function and the boundary conditions are the only elements needed for quantum threshold reflection. In this section we present a detailed investigation of the threshold dynamics for the one-dimensional Morse potential and a smooth Eckart step potential [26,27]. In what follows the particle is taken to be incident from the right rather than from the left as in the preceding section.

The Schrödinger equation for the scattering of a particle of mass m and incident energy $E_i = \hbar^2 k^2 / 2m$ (with initial momentum $\hbar k$) by a Morse potential is

$$-\frac{\hbar^2}{2m} \frac{d^2 \Psi(z)}{dz^2} + V \left[\exp\left(-2\frac{z-z_0}{d}\right) - 2 \exp\left(-\frac{z-z_0}{d}\right) \right] \Psi(z) = \frac{\hbar^2 k^2}{2m} \Psi(z), \quad (3.1)$$

where V is the well depth, d^{-1} is the stiffness parameter, the minimum of the potential is located at $z = z_0$, and the harmonic frequency of motion about the well bottom is

$$\omega_0^2 = \frac{2V}{md^2}. \quad (3.2)$$

Introducing the dimensionless “coordinate” [26,28]

$$y = Y \exp\left(-\frac{z-z_0}{d}\right) \quad (3.3)$$

and the reduced variables

$$\mu^2 = -d^2 k^2, \quad 1 = \frac{8md^2 V}{\hbar^2 Y^2}, \quad (3.4)$$

where the parameter Y is expressed in terms of the other parameters, allows us to rewrite the Schrödinger equation (3.1) as

$$\frac{1}{y} \frac{d\Psi(y)}{dy} + \frac{d^2 \Psi(y)}{dy^2} + \left[-\frac{1}{4} + \frac{Y}{2y} - \frac{\mu^2}{y^2} \right] \Psi(y) = 0. \quad (3.5)$$

Using the substitution

$$\Psi(y) = y^\mu \exp\left(-\frac{y}{2}\right) u(y) \quad (3.6)$$

leads to the differential equation for the confluent hypergeometric function [29]

$$y \frac{d^2 u(y)}{dy^2} + (1 + 2\mu - y) \frac{du(y)}{dy} - \left(\frac{1 + 2\mu - Y}{2} \right) u(y) = 0. \quad (3.7)$$

Its two independent solutions u and v may be chosen to be

$$u(y) = M\left(\frac{1 + 2\mu - Y}{2}, 1 + 2\mu, y\right), \quad (3.8)$$

$$v(y) = y^{-2\mu} M\left(\frac{1 - 2\mu - Y}{2}, 1 - 2\mu, y\right),$$

where M is Kummer’s function as defined in Ref. [29].

The scattering wave functions are a linear combination of the two independent solutions

$$\Psi^+(y) = y^\mu \exp\left(-\frac{y}{2}\right) [Au(y) + Bv(y)]. \quad (3.9)$$

To determine the coefficients one imposes the boundary conditions. (As already noted above, here our convention is that the particle is incident from the right and not from the left as in the preceding section.) When $z \rightarrow \infty$ with $k > 0$, the scattering wave function has the form

$$\Psi^+(z) = \frac{1}{\sqrt{2\pi}} [\exp(-ikz) + R(k) \exp(ikz)] \quad (3.10)$$

and $R(k)$ is the reflection amplitude. The second boundary condition is that the wave function vanishes in the limit $z \rightarrow -\infty$. These boundary conditions are another indication that the full potential region is needed to correctly extract the reflection amplitude, not only its long tail.

Noting the asymptotic property of the Kummer function

$$\lim_{y \rightarrow 0} M\left(\frac{1 + 2\mu - Y}{2}, 1 + 2\mu, y\right) = 1, \quad (3.11)$$

we find that when $z \rightarrow \infty$,

$$\begin{aligned} \lim_{z \rightarrow \infty} \Psi^+(z) &= Ay^\mu + By^{-\mu} \\ &= AY^{ikd} \exp(ikz_0) \left[\exp[-ik(z-z_0)] + \frac{B}{A} Y^{-2ikd} \right. \\ &\quad \left. \times \exp(ikz) \exp(-2ikz_0) \right], \end{aligned} \quad (3.12)$$

from which we identify the reflection amplitude

$$R(k) = \frac{B}{A} \exp(-2ikz_0) Y^{-2ikd} \quad (3.13)$$

and its modulus or reflectivity as $|R| = |B/A|$.

The second boundary condition is for $z \rightarrow -\infty$ or equivalently $y \rightarrow \infty$. Noting the properties

$$\begin{aligned} \lim_{y \rightarrow \infty} M\left(\frac{1 + 2\mu - Y}{2}, 1 + 2\mu, y\right) &= \frac{\Gamma(1 + 2\mu)}{\Gamma(\frac{1+2\mu-Y}{2})} \exp(y) y^{(-1-2\mu-Y)/2}, \end{aligned} \quad (3.14)$$

$$\begin{aligned} \lim_{y \rightarrow \infty} y^{-2\mu} M\left(\frac{1 - 2\mu - Y}{2}, 1 - 2\mu, y\right) &= \frac{\Gamma(1 - 2\mu)}{\Gamma(\frac{1-2\mu-Y}{2})} \exp(y) y^{(-1-2\mu-Y)/2} \end{aligned} \quad (3.15)$$

and imposing the boundary condition that the wave function vanishes when $z \rightarrow -\infty$ implies that the reflection amplitude

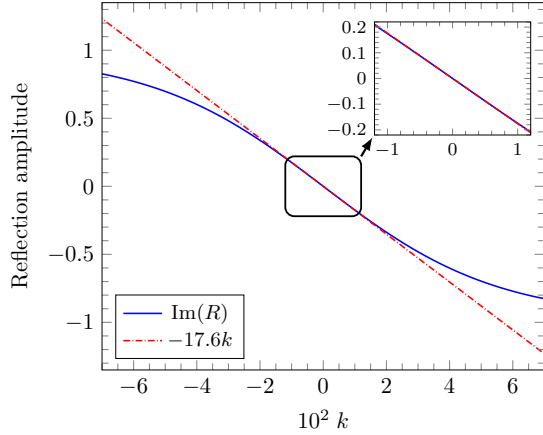


FIG. 1. Imaginary part of the reflection amplitude as a function of k . The region around $k = 0$ is magnified.

is given by

$$R(k) = -\frac{\Gamma(1+2\mu)\Gamma\left(\frac{1-2\mu-Y}{2}\right)}{\Gamma(1-2\mu)\Gamma\left(\frac{1+2\mu-Y}{2}\right)} \exp(-2ikz_0)Y^{-2ikd}. \quad (3.16)$$

From these results one notes that, as expected, $R^*(k) = R(-k)$ and $|R(k)|^2 = 1$. In the context of quantum threshold reflection we readily establish that in this limit

$$\lim_{k \rightarrow 0} R(k) \exp(2ikz_0) = -1 + 2idk \left[\ln(Y) + d\bar{\Psi}\left(\frac{1+Y}{2}\right) - \pi \tan\left(\frac{\pi Y}{2}\right) + 4\gamma \right], \quad (3.17)$$

where $\bar{\Psi}$ is the digamma function and $\gamma = 0.5772\dots$ is Euler's constant.

To exemplify the quantum reflection threshold region we plot in Fig. 1 the imaginary part of the reflection amplitude as a function of k . For this purpose, and throughout this paper, all numerical results are given in atomic units, with $\hbar = m = 1$, and the parameters of the Morse potential are taken to be $V = 1$, $d = 1$, and $z_0 = 0$ so that $\omega_0 = \sqrt{2}$ and $Y = 2\sqrt{2}$. We note the linear dependence of the imaginary part of the amplitude about $k = 0$. The numerical slope is -17.626 [see also Eq. (3.17)]. The interval of linearity is roughly $[-10^{-2} \leq k \leq 10^{-2}]$ and this is the domain of quantum threshold reflection for the Morse potential (using the parameters as above).

This range of k values is also the region in which the absolute value of the badlands function for the Morse potential becomes greater than unity. Defining the classical momentum as

$$p(z) = \pm\sqrt{2m[E - V(z)]}, \quad (3.18)$$

the badlands function is defined as [9]

$$Q(z) = \hbar^2 \left(\frac{3}{4} \frac{(p')^2}{p^4} - \frac{p''}{2p^3} \right), \quad (3.19)$$

where primes denote derivatives with respect to the argument. In Fig. 2 we plot the absolute value of the badlands function vs the coordinate z in the range of k values for which the scattering is dominated by quantum threshold reflection. As expected, the Morse potential exhibits a badlands region, the

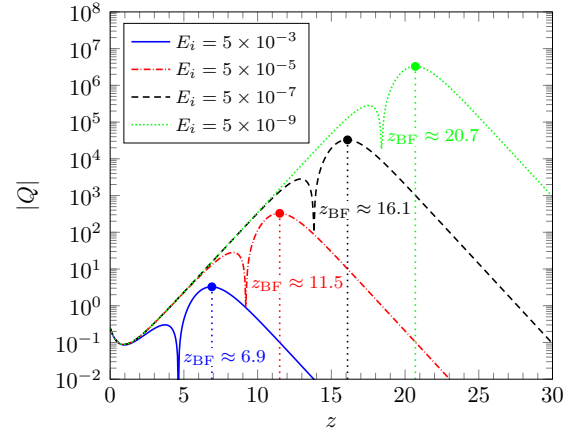


FIG. 2. Absolute value of the badlands function $|Q|$ as a function of the distance z for various incident energies. The badlands region is localized around the value z_{BF} where $|Q|$ attains its maximal value. The lines labeled with $z_{BF} = 6.9, 11.5, 16.1, 20.7$ correspond to the incident energies $E_i = 5 \times 10^{-3}, 5 \times 10^{-5}, 5 \times 10^{-7}, 5 \times 10^{-9}$, respectively.

location of the regions in which $|Q(z)| > 1$ moves outward, and the magnitude of the function increases with decreasing k .

Imposing the boundary condition for $z \rightarrow \infty$ allows us to identify that

$$A \exp(ikz_0)Y^{ikd} = \frac{1}{\sqrt{2\pi}}, \quad (3.20)$$

so the final expression for the scattering wave function for a given value of the incident momentum $\hbar k$ is

$$\begin{aligned} \langle z|k^+ \rangle \equiv \Psi_k^+(z) &= \frac{1}{\sqrt{2\pi}} \exp\left(-\frac{y}{2}\right) \\ &\times \left[\exp(-ikz)M\left(\frac{1+2ikd-Y}{2}, 1+2\mu, y\right) \right. \\ &\left. + R(k) \exp(ikz)M\left(\frac{1-2ikd-Y}{2}, 1-2ikd, y\right) \right]. \end{aligned} \quad (3.21)$$

This result will be used in the next section to construct the propagator for the Morse potential.

B. Time domain: Wave-packet propagation

For the scattering from the Morse potential, there is no transmission so that the completeness of the scattering states is expressed as

$$\hat{I} = \int_0^\infty dk |k^+ \rangle \langle k^+|. \quad (3.22)$$

The coordinate space matrix element of the propagator is then

$$\left\langle z \left| \exp\left(-\frac{i\hat{H}t}{\hbar}\right) \right| z' \right\rangle = \int_0^\infty dk \exp\left(-i\frac{\hbar k^2}{2m}t\right) \langle z|k^+ \rangle \langle k^+|z' \rangle. \quad (3.23)$$

We will study the spatial and temporal dynamics of an initial coherent state centered about the position z_i and incident

momentum $-p_i$ ($p_i > 0$) and characterized by the width parameter Γ . Its coordinate representation is

$$\langle z|\Phi\rangle = \left(\frac{\Gamma}{\pi}\right)^{1/4} \exp\left(-\Gamma\frac{(z-z_i)^2}{2} + \frac{i}{\hbar}p_i(z_i-z)\right). \quad (3.24)$$

Since the incident wave function is localized in the asymptotic region, we may readily evaluate the matrix element $\langle k^+|\Phi\rangle$ using the asymptotic form of the wave function

$$\langle k^+|\Phi\rangle = \left(\frac{1}{\pi\Gamma}\right)^{1/4} \left\{ \exp\left[ikz_i - \frac{1}{2\Gamma}\left(\frac{p_i}{\hbar} - k\right)^2\right] + R^*(k) \exp\left[-ikz_i - \frac{1}{2\Gamma}\left(\frac{p_i}{\hbar} + k\right)^2\right] \right\}. \quad (3.25)$$

The time evolution of the incident wave packet is then given by

$$\begin{aligned} \left\langle z \left| \exp\left(-\frac{i\hat{H}t}{\hbar}\right) \right| \Phi \right\rangle &= \int_0^\infty dk \exp\left(-i\frac{\hbar k^2}{2m}t\right) \langle z|k^+\rangle \langle k^+|\Phi\rangle \\ &= \left(\frac{1}{\pi\Gamma}\right)^{1/4} \frac{1}{\sqrt{2\pi}} \exp\left[-\frac{Y}{2} \exp\left(-\frac{z-z_0}{d}\right)\right] \\ &\quad \times \left\{ \int_{-\infty}^\infty dk \exp\left[-i\frac{\hbar k^2}{2m}t - \frac{1}{2\Gamma}\left(\frac{p_i}{\hbar} - k\right)^2 - ik(z-z_i)\right] M\left(\frac{1+2ikd-Y}{2}, 1+2ikd, y(z)\right) \right. \\ &\quad \left. + \int_{-\infty}^\infty dk \exp\left[-i\frac{\hbar k^2}{2m}t - \frac{1}{2\Gamma}\left(\frac{p_i}{\hbar} - k\right)^2 + ik(z+z_i)\right] R(k) M\left(\frac{1-2ikd-Y}{2}, 1-2ikd, y(z)\right) \right\}, \quad (3.26) \end{aligned}$$

where we used the fact that $R^*(k) = R(-k)$. With these preliminaries, the time propagation is reduced to a numerical quadrature over k . In practice, the propagation of this initial wave packet expressed in Eq. (3.26) is carried out by integration over k in the range $[p_i/\hbar - 7\sqrt{\Gamma}; p_i/\hbar + 7\sqrt{\Gamma}]$. The overlap $|\langle k^+|\Phi\rangle|$ is virtually zero outside this range. The number of k -grid points is 5×10^4 and this leads to converged evaluation of the integral in Eq. (3.26) for any combination of E_i , Γ , t , and z used in this study.

The time evolution of the initial wave packet is plotted in Figs. 3, 4, and 5 for three different incident energies ($E_i = p_i^2/2$) 5×10^{-1} , 5×10^{-5} , and 5×10^{-9} , respectively. The initial parameters for the three energies are $(-p_i, z_i) = (-1, 10^2)$ and $\Gamma = 10^{-2}$, $(-p_i, z_i) = (-10^{-2}, 10^4)$ and $\Gamma = 10^{-6}$, and $(-p_i, z_i) = (-10^{-4}, 10^6)$ with $\Gamma = 10^{-10}$, respectively. Four panels are displayed in each figure. Figures 3(a), 4(a), and 5(a) show the quantum time evolution of the probability density of the coherent state evaluated from Eq. (3.26). Figures 3(b), 4(b), and 5(b) show the corresponding time evolution of $|\langle z|\Phi\rangle|^2$ based on a classical Wigner dynamics approximation to the exact quantum dynamics. In the classical Wigner propagation, classical trajectories are launched with initial conditions sampled from the Wigner transform of $\langle z|\Phi\rangle$ (in all cases 4×10^9 trajectories are included) and the relative probability density at z' and t' is calculated by counting the trajectories with position z' at time t' . Figures 3(c), 4(c), and 5(c) and Figs. 3(d), 4(d), and 5(d) show a close-up of the time-dependent probability density close to the well of the Morse potential for the exact quantum and classical Wigner dynamics, respectively. In all panels, the number of grid points in both z and t space is 2000.

In Fig. 3 the dotted line (denoted by z_0) shows the location of the Morse potential well and the dash-dotted line (denoted by z_{TP}) shows the location of the classical turning point at the incident momentum p_i . In this relatively-high-energy case, the magnitude of the badlands function remains small so that in any case it is not important. In Figs. 4 and 5 the dotted line

(denoted by z_{BF}) shows the location of the maximal magnitude of absolute value of the badlands function.

As shown in Fig. 3 at the highest energy probed ($E_i = 0.5$), which is at the edge of the region in which the imaginary part of the reflection amplitude is still linear in k (see Fig. 1), the quantum wave packet reaches the left turning point of the Morse potential and even penetrates into the classically forbidden region. For the classical Wigner approximation, the probability density builds up at the classical turning point z_{TP} (with a slight “penetration” due to the momentum spread around p_i of the Wigner transform of $\langle z|\Phi\rangle$) and has a relatively small amplitude at the bottom of the potential well, where the classical trajectories spend less time. Note that even at this relatively high energy, there is a qualitative difference between the quantum and classical Wigner scattering. The former shows an oscillatory structure typical for the interference of incoming and outgoing waves, while the incoherent Wigner distribution does not show this at all.

At the two lower incident energies shown in Figs. 4 and 5, the quantum wave packet does not reach the interaction region and the reflection takes place at distances that are far greater than z_{BF} , where the maximum of the absolute value of the badlands function is found. From these two plots it becomes evident that the badlands region has no special meaning for the quantum evolution. Especially at the lowest energy probed (Fig. 5), the first maximal density is located at a distance which is ~ 1000 times larger than the location of the maximum of the badlands function (z_{BF}). No special attention should then be paid to the badlands function. The repulsive wall of the potential or its left turning point also plays no role in this coherent interference process except for imposing the boundary condition that the function vanishes to the left of the repulsive wall. On the other hand, the classical Wigner approximation of the wave-packet dynamics leads to a significant probability density even at the badlands region. This is not surprising since the badlands region is positioned in the tail of the Morse

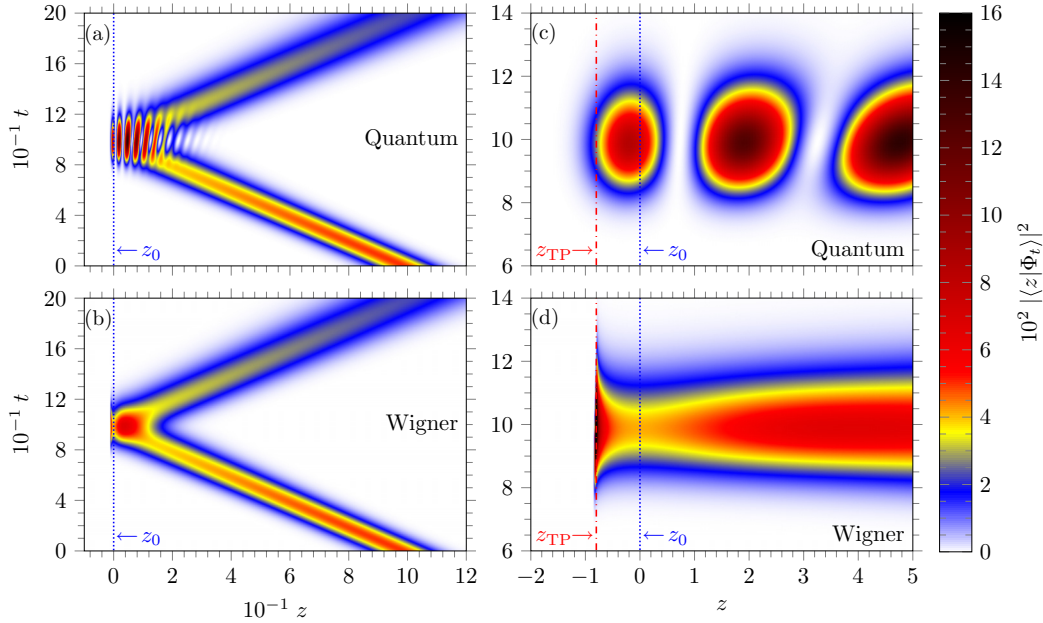


FIG. 3. Space and time evolution of a coherent state scattered from a Morse potential at the incident energy $E_i = 0.5$. The time and space evolutions of the probability density are shown using (a) exact quantum and (b) classical Wigner propagation. (c) and (d) Close-up of the same time evolutions close to the potential well, respectively. The minimum of the Morse potential z_0 and the classical turning point z_{TP} (corresponding to E_i) are indicated. At this relatively high energy the quantum wave packet approaches the repulsive wall and even tunnels beyond it. For further details see the text.

potential, where the potential is almost constant. Hence, the time spent by the classical trajectories in this region is not different from the remaining part of the potential tail.

As may also be inferred from Figs. 4 and 5, the quantum reflection is just a result of the coherent interference of the incoming and outgoing wave functions. Since the particle is

almost a free particle, the boundary condition that the wave function vanishes a bit further left to the classical turning point implies that to a good approximation the wave function is just $\sim \sin[k(z - z_{TP})]$, which is just the difference between the amplitude of the incoming and outgoing waves. Inspection of the two figures shows that at the respective inflection times

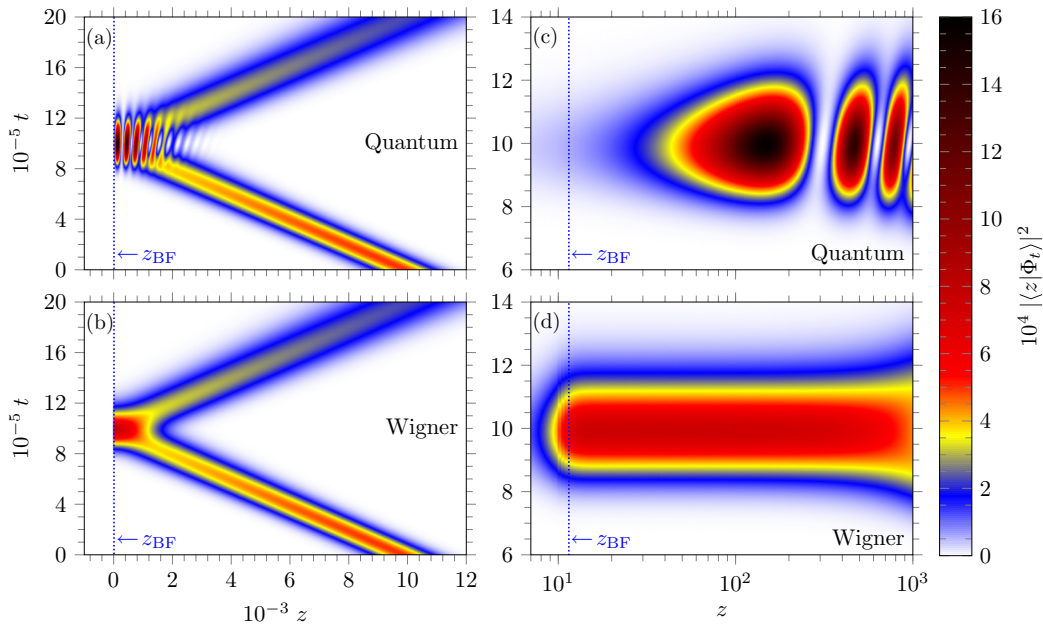


FIG. 4. Space and time evolution of a coherent state scattered from a Morse potential at the incident energy $E_i = 5 \times 10^{-5}$. The time and space evolutions of the probability density are shown using (a) exact quantum and (b) classical Wigner propagation. (c) and (d) Close-up of the same time evolutions close to the potential well, respectively. The maximum of the absolute value of the badlands function $|Q(z)|$ at this incident energy is at $z_{BF} \approx 11.5$.

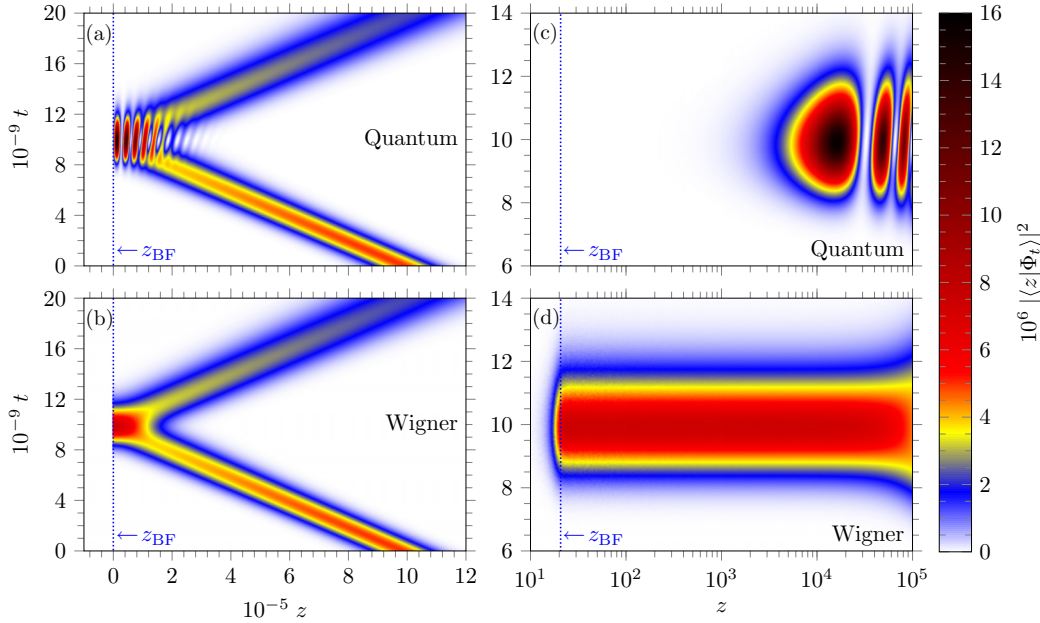


FIG. 5. Space and time evolution of a coherent state scattered from a Morse potential at the incident energy $E_i = 5 \times 10^{-9}$. The time and space evolutions of the probability density are shown using (a) exact quantum and (b) classical Wigner propagation. (c) and (d) Close-up of the same time evolutions close to the potential well, respectively. The maximum of the absolute value of the badlands function $|Q(z)|$ at this incident energy is at $z_{\text{BF}} \approx 20.7$.

$t = 10^6, 10^{10}$ the maximum of the wave function in the two respective figures occurs at $z - z_{\text{TP}} \simeq \pi/2k_i$ while the first zero occurs at $z - z_{\text{TP}} \simeq \pi/k_i$. Changing the location of the turning point, for example, by making the Morse potential softer, would change the location of the respective maxima. This is again another indication of the nonlocal character of this scattering or coherent interference process.

C. Mean flight time

In this section we will compare the mean flight time of the initial wave packet for arrival at a position $y = 2z_i$ as derived from the exact quantum mechanics and a classical Wigner approximation. For this purpose, we note that the transition path time distribution [30], in a quantum mechanical context, is defined in terms of the positive density correlation function at time t about the final position y ,

$$C_t(y; \Phi) = \text{Tr}[|\Phi\rangle\langle\Phi| \hat{K}_t^\dagger \delta(\hat{z} - y) \hat{K}_t] = |\langle y | \hat{K}_t | \Phi \rangle|^2, \tag{3.27}$$

TABLE I. Mean flight time associated with quantum threshold reflection. Here E_i is the incident energy, $(-p_i, z_i)$ is the phase-space center of $\langle z | \Phi \rangle$, and Γ is its width parameter; $y = 2z_i$ is the position at which the transition path time distribution is evaluated; and z_{TP} is the classical turning point corresponding to E_i ; t_{cl} is the time it takes the classical particle, moving on the Morse potential with initial conditions $(-p_i, z_i)$, to reach y ; $\langle t \rangle_{\text{free}}$ is the mean flight time for a free particle to traverse the distance $y + z_i + 2|z_{\text{TP}}|$ at the incident energy; $\langle t \rangle_{\text{QM}}$ is the mean flight time for arrival at y based on exact propagation of $\langle z | \Phi \rangle$; $\langle t \rangle_{\text{W}}$ is the mean flight time for arrival at y based on classical Wigner propagation of $\langle z | \Phi \rangle$. The relative error in the classical Wigner computation is less than 10^{-4} .

| E_i | $(-p_i, z_i)$ | Γ | z_{TP} | t_{cl} | $\langle t \rangle_{\text{free}}$ | $\langle t \rangle_{\text{QM}}$ | $\langle t \rangle_{\text{W}}$ |
|--------------------|--------------------|------------|-----------------|------------------------|-----------------------------------|---------------------------------|--------------------------------|
| 5×10^{-1} | $(-1, 10^2)$ | 10^{-2} | -0.799642 | 2.995945×10^2 | 3.015993×10^2 | 3.027164×10^2 | 3.024703×10^2 |
| 5×10^{-3} | $(-10^{-1}, 10^3)$ | 10^{-4} | -0.694295 | 2.990785×10^2 | 3.001389×10^4 | 3.035366×10^4 | 3.019901×10^4 |
| 5×10^{-5} | $(-10^{-2}, 10^4)$ | 10^{-6} | -0.693160 | 2.998158×10^2 | 3.000139×10^6 | 3.032529×10^6 | 3.027396×10^6 |
| 5×10^{-7} | $(-10^{-3}, 10^5)$ | 10^{-8} | -0.693147 | 2.999724×10^2 | 3.000014×10^8 | 3.030957×10^8 | 3.028983×10^8 |
| 5×10^{-9} | $(-10^{-4}, 10^6)$ | 10^{-10} | -0.693147 | 2.999963×10^2 | 3.000001×10^{10} | 3.030797×10^{10} | 3.029225×10^{10} |

where $\hat{K}_t = \exp(-i\hat{H}t/\hbar)$ is the quantum propagator [31–34]. The transition path time probability distribution reads

$$P_t(y; \Phi) = \frac{C_t(y; \Phi)}{\int_0^\infty dt C_t(y; \Phi)}, \tag{3.28}$$

where we assume that the normalization integral $\int_0^\infty dt C_t(y; \Phi)$ is finite. The mean flight time for arrival at y is then, by definition,

$$\langle t \rangle_{\text{QM}} = \int_0^\infty dt t P_t(y; \Phi). \tag{3.29}$$

The correlation function of Eq. (3.27) can be rewritten as a phase-space trace of two Wigner densities. One is the Wigner representation of $\langle z | \Phi \rangle$ and the other is the Wigner representation of the Heisenberg time evolved density $\hat{\rho}(t) = \exp(i\hat{H}t)\delta(\hat{z} - y)\exp(-i\hat{H}t)$. The classical Wigner approximation is then obtained by replacing the exact Wigner representation of the time-evolved quantum density with its classical Wigner approximation $\delta(q_t - y)$, where q_t is the classical

TABLE II. Mean flight time associated with quantum threshold reflection for different width parameters of the initial wave packet. All notation is as in Table I.

| E_i | $(-p_i, z_i)$ | Γ | z_{TP} | t_{cl} | $\langle t \rangle_{\text{free}}$ | $\langle t \rangle_{\text{QM}}$ | $\langle t \rangle_{\text{W}}$ |
|--------------------|--------------------|------------|-----------------|---------------------------|-----------------------------------|---------------------------------|--------------------------------|
| 5×10^{-1} | $(-1, 10^3)$ | 10^{-2} | -0.799642 | 2.999595×10^3 | 3.001599×10^3 | 3.030568×10^3 | 3.030314×10^3 |
| 5×10^{-1} | $(-1, 10^3)$ | 10^{-3} | -0.799642 | 2.999595×10^3 | 3.001599×10^3 | 3.002835×10^3 | 3.002590×10^3 |
| 5×10^{-1} | $(-1, 10^3)$ | 10^{-4} | -0.799642 | 2.999595×10^3 | 3.001599×10^3 | 3.000132×10^3 | 2.999874×10^3 |
| 5×10^{-9} | $(-10^{-4}, 10^7)$ | 10^{-10} | -0.693147 | 2.999996×10^{11} | 3.000000×10^{11} | 3.030856×10^{11} | 3.030788×10^{11} |
| 5×10^{-9} | $(-10^{-4}, 10^7)$ | 10^{-11} | -0.693147 | 2.999996×10^{11} | 3.000000×10^{11} | 3.003084×10^{11} | 3.003007×10^{11} |
| 5×10^{-9} | $(-10^{-4}, 10^7)$ | 10^{-12} | -0.693147 | 2.999996×10^{11} | 3.000000×10^{11} | 3.000377×10^{11} | 3.000296×10^{11} |

trajectory that is evolved to time t from the initial condition (p, q) . This enables us to calculate the mean flight time based on the classical Wigner approximation, which we denote by $\langle t \rangle_{\text{W}}$.

The resulting mean flight times as a function of the incident energy are shown in Table I. First we notice that the mean flight times based on the classical Wigner approximation are consistently smaller than the corresponding times based on exact quantum propagation. Naively, this might not be expected from visual inspection of Figs. 4 and 5, which show that the quantum probability density in the neighborhood of the potential well is much smaller than the Wigner probability density [25]. In different words, if the quantum reflection phenomenon would be a result of reflection from the badlands region, the mean flight time of the quantum particle should be *less* than that of the classical Wigner flight time since the path traversed is shorter. The fact that $\langle t \rangle_{\text{W}} < \langle t \rangle_{\text{QM}}$ indicates that the quantum particle is not being reflected far away from the potential well. Furthermore, the mean flight time of the free (classical) particle for traversal of the distance $y + z_i + 2|z_{\text{TP}}|$, where z_{TP} is the classical turning point corresponding to E_i , is consistently shorter [8] than either $\langle t \rangle_{\text{QM}}$ or $\langle t \rangle_{\text{W}}$.

At first sight, one would wonder, though, why the classical Wigner times are longer than the free particle time. The well potential accelerates the classical particle so that the classical Wigner flight time should be shorter than that of the free particle. The reason for this has to do with the Gaussian nature of the incident wave packet. The free particle time does not take this Gaussian structure into consideration; it is the free particle time for a single trajectory at the mean energy of the incident wave packet. To clarify this we present in Table II the mean flight times as a function of the width parameter of the initial wave packet for two incident energies. In the higher-energy case, quantum reflection is not important, but it dominates the lower-energy case. When the width parameter is decreased, the momentum spread of the initial wave packet is decreased. In this higher-energy case, the inequality $\langle t \rangle_{\text{W}} < \langle t \rangle_{\text{QM}}$ holds for all three width parameters, but when the width is sufficiently small ($\Gamma = 10^{-4}$), both mean flight times become shorter than the corresponding free particle flight time

$\langle t \rangle_{\text{free}}$. However, they are consistently longer than the time it takes the classical particle, moving on the Morse potential with initial conditions $(-p_i, z_i)$, to reach y (denoted by t_{cl} in Table II). It becomes clear then that the Gaussian averaging leads to flight times that are slightly longer than expected for a single energy due to the momentum distribution of the incident wave packet. Different incident momenta have slightly different turning points and thus different flight times. The Gaussian averaging is thus not trivial.

To summarize, the time-dependent analysis has shown that the quantum flight time is very similar to the classical Wigner flight time even when quantum threshold reflection dominates the dynamics. Moreover, the quantum time is even slightly longer than the classical Wigner time, negating the claim such as the one in Ref. [25] that the “the quantum particle spends less time in the interaction region than the classical particle.” The badlands region does not shorten the quantum time as compared to the classical.

D. Quantum threshold reflection for the smooth Eckart potential step

To complete the picture and prevent any misconception arising from the fact that the reflection probability from a Morse potential is always unity we also consider the case of scattering from a smooth potential step. For this purpose we use the Eckart potential [27]

$$V_{\text{E}}(z) = V \left(\frac{1}{1 + \exp(z/\beta)} + \frac{\kappa \exp(z/\beta)}{[1 + \exp(z/\beta)]^2} \right), \quad (3.30)$$

with $\kappa = 1/3$ such that the potential is a smooth step with height $|V|$, and the reflection probability is now dependent on the incident energy (in the following $V = -1$ a.u. and $\beta = 1$ a.u.). The potential step is plotted in Fig. 6. The wave-packet propagation is carried out using the method described in Sec. III B, where the appropriate transmission and reflection amplitudes and scattering states of the Eckart potential are used.

The transmission and reflection amplitudes at an incident energy E (for a particle coming from the right) are given by [27]

$$T_{\text{E}}(k) = \frac{\Gamma(\frac{1}{2} + \omega - i\beta k - i\beta k')\Gamma(\frac{1}{2} - \omega - i\beta k - i\beta k')}{\Gamma(1 - 2i\beta k)\Gamma(-2i\beta k')} \sqrt{\frac{k}{k'}}, \quad (3.31)$$

$$R_{\text{E}}(k) = \frac{\Gamma(\frac{1}{2} + \omega - i\beta k - i\beta k')\Gamma(\frac{1}{2} - \omega - i\beta k - i\beta k')\Gamma(2i\beta k')}{\Gamma(\frac{1}{2} + \omega - i\beta k + i\beta k')\Gamma(\frac{1}{2} - \omega - i\beta k + i\beta k')\Gamma(-2i\beta k')}, \quad (3.32)$$

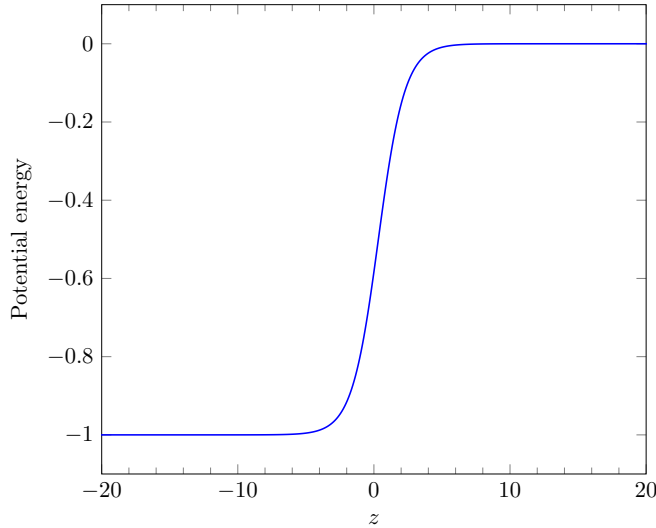


FIG. 6. The Eckart potential as a function of the position z , using the parameters $\kappa = 1/3$, $V = -1$ a.u., and $\beta = 1$ a.u.

where $\hbar k = \sqrt{2mE}$, $\hbar k' = \sqrt{2m(E - V)}$, and $4\omega^2 = 1 - 8mV\beta^2\kappa/\hbar^2$, and the general scattering state can be

written as

$$\langle z|k^+\rangle = \sqrt{\frac{k'}{k}} \frac{T_E}{\sqrt{2\pi}} \tilde{z}^{i\beta k'} (1 - \tilde{z})^{-i\beta k} F\left(\frac{1}{2} + \omega - i\beta k + i\beta k', \frac{1}{2} - \omega - i\beta k + i\beta k'; 1 - 2i\beta k, 1 - \tilde{z}\right), \quad (3.33)$$

using the auxiliary variable $\tilde{z} = 1/[1 + \exp(-z/\beta)]$. Here F denotes Gauss's hypergeometric function. As for the Morse potential, the overlap $\langle k^+|\Phi\rangle$ between a scattering state and the initial wave packet can be evaluated analytically using the asymptotic form of Eq. (3.33) and the wave-packet propagation is readily computed using the same quadrature procedure as described for the Morse potential.

In Fig. 7 the time evolution of the initial wave packet [as in Eq. (3.24)], on the Eckart potential, is shown for the parameters used in Fig. 5 [$(-p_i, z_i) = (-10^{-4}, 10^6)$ and $\Gamma = 10^{-10}$]. Based on visual inspection of Figs. 5 and 7, the time evolutions of the initial wave packet on the two potentials seem identical. There are tiny numerical differences between the two densities, since the quantum reflection on the Eckart potential is not total (the reflection probability is 99.9% for the chosen parameters). In the case of the Eckart step potential, the location of the maximum value of the badlands function $|Q|$ is at $z_{\text{BF}} \approx 20.3$ [see Fig. 7(c)]. Thus, the same conclusion regarding the role of the badlands region is reached for quantum threshold reflection on the smooth Eckart step potential.

IV. CONCLUSION

In this work we have clearly shown that there is no need to invoke the nonclassical or badlands region of the interaction potential to understand the phenomenon of quantum threshold reflection. At the threshold energies, imposing the condition that the wave function vanishes beyond the classical turning point of the potential implies that the scattering wave function is well approximated as $\sin[k(z - z_{\text{TP}})]$. Since the incident wave vector is very small, the first maximum of the wave function occurs far away from the turning point. As a result, the density around the potential well is very small and any interaction with the surface is negligible. A comparison with results based on a classical Wigner approximation serves to stress that quantum reflection is a result of the coherent sum of an incoming and an outgoing wave and it is the destructive and constructive interference that combines to give a density which is very small in the strong interaction region. This is why, for example, the He dimer does not dissociate upon scattering from a surface at very low energies. This has nothing to do with the badlands region.

Quantum threshold reflection is thus a nonlocal interference process, in which the incoming and outgoing waves interfere destructively in the region of strong interaction, due to the boundary condition that the wave function must vanish beyond the classical turning point region. The badlands region has implications when attempting to construct a WKB solution

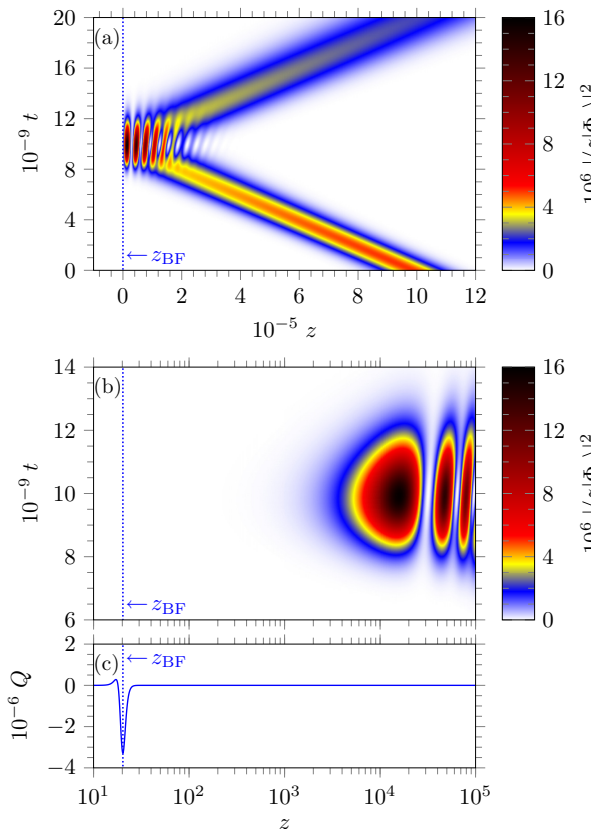


FIG. 7. (a) Space and time evolution of a coherent state scattered from a smooth Eckart step potential at the incident energy $E_i = 5 \times 10^{-9}$. In this case the reflection probability is $|R|_{\Phi}^2 \approx 99.9\%$. (b) Close-up of the same time evolution close to the potential step. The maximum of the absolute value of the badlands function $|Q(z)|$ at this incident energy is at $z_{\text{BF}} \approx 20.3$.

to the scattering wave function, but it has no implication on the evolution of the quantum density, neither in space nor in time. This study should serve to definitely rule out the badlands region as a criterion for quantum threshold reflection.

ACKNOWLEDGMENTS

This work was supported by a grant from the Israel Science Foundation and was partially supported by Grant No. FIS2014-52172-C2-1-P from the Ministerio de Economía y Competitividad (Spain).

-
- [1] P. Senn, *Am. J. Phys.* **56**, 916 (1988).
 - [2] J. E. Lennard-Jones and A. F. Devonshire, *Proc. R. Soc. London Ser. A* **156**, 6 (1936).
 - [3] W. Kohn, *Surf. Rev. Lett.* **1**, 129 (1994).
 - [4] R. Côté, E. J. Heller, and A. Dalgarno, *Phys. Rev. A* **53**, 234 (1996).
 - [5] A. Mody, M. Haggerty, J. M. Doyle, and E. J. Heller, *Phys. Rev. B* **64**, 085418 (2001).
 - [6] H. Friedrich and J. Trost, *Phys. Rep.* **397**, 359 (2004).
 - [7] H. Friedrich, G. Jacoby, and C. G. Meister, *Phys. Rev. A* **65**, 032902 (2002).
 - [8] H. Friedrich and A. Jurisch, *Phys. Rev. Lett.* **92**, 103202 (2004).
 - [9] H. Friedrich, *Scattering Theory*, Lecture Notes in Physics Vol. 872 (Springer, Berlin, 2013), p. 210.
 - [10] B. A. Stickler, U. Even, and K. Hornberger, *Phys. Rev. A* **91**, 013614 (2015).
 - [11] A. R. Barnea, B. A. Stickler, O. Cheshnovsky, K. Hornberger, and U. Even, *Phys. Rev. A* **95**, 043639 (2017).
 - [12] R. B. Doak and A. V. G. Chizmeshya, *Europhys. Lett.* **51**, 381 (2000).
 - [13] W. Zhang, J. H. Lee, H. A. Kim, B. G. Jin, B. J. Kim, L. Y. Kim, B. S. Zhao, and W. Schöllkopf, *Phys. Chem. Chem. Phys.* **17**, 3670 (2016).
 - [14] G. Dufour, R. Guérout, A. Lambrecht, and S. Reynaud, *Europhys. Lett.* **110**, 30007 (2015).
 - [15] G. Dufour, R. Guérout, A. Lambrecht, and S. Reynaud, *J. Phys. B* **48**, 155002 (2015).
 - [16] S. Miret-Artés and E. Pollak, *J. Phys. Chem. Lett.* **8**, 1009 (2017).
 - [17] B. S. Zhao, S. A. Schulz, S. A. Meek, G. Meijer, and W. Schöllkopf, *Phys. Rev. A* **78**, 010902(R) (2008).
 - [18] B. S. Zhao, G. Meijer, and W. Schöllkopf, *Science* **331**, 892 (2011).
 - [19] T. Seideman and W. H. Miller, *J. Chem. Phys.* **96**, 4412 (1992).
 - [20] J. G. Muga, J. P. Palao, B. Navarro, and I. L. Egusquiza, *Phys. Rep.* **395**, 357 (2004).
 - [21] B. Herwerth, M. DeKieviet, J. Madroñero, and S. Wimberger, *J. Phys. B* **46**, 141002 (2013).
 - [22] E. Galiffi, C. Sünderhauf, M. DeKieviet, and S. Wimberger, *J. Phys. B* **50**, 095001 (2017).
 - [23] E. J. Heller, *J. Chem. Phys.* **65**, 1289 (1976).
 - [24] B. R. McQuarrie, D. G. Abrashkevich, and P. Brumer, *J. Chem. Phys.* **119**, 3606 (2003).
 - [25] D. P. Clougherty and W. Kohn, *Phys. Rev. B* **46**, 4921 (1992).
 - [26] P. M. Morse, *Phys. Rev.* **34**, 57 (1929).
 - [27] *Propagators in Quantum Chemistry*, 2nd ed., edited by J. Linderberg and Y. Öhrn (Wiley, New York, 2004).
 - [28] A. Matsumoto, *J. Phys. A: At. Mol. Opt. Phys.* **21**, 2863 (1988).
 - [29] M. Abramowitz and I. A. Stegun, *Handbook of Mathematical Functions* (Dover, New York, 1972).
 - [30] G. Hummer, *J. Chem. Phys.* **120**, 516 (2004).
 - [31] E. Pollak, *J. Phys. Chem. Lett.* **8**, 352 (2017).
 - [32] E. Pollak, *Phys. Rev. Lett.* **118**, 070401 (2017).
 - [33] E. Pollak, *Phys. Rev. A* **95**, 042108 (2017).
 - [34] J. Petersen and E. Pollak, *J. Phys. Chem. Lett.* **8**, 4017 (2017).